A High-Frequency SSVEP-BCI System Based on Simultaneous Modulation of Luminance and Motion Using Intermodulation Frequencies

Meng Li, Xiaogang Chen, *Member, IEEE*, and Hongyan Cui

***Abstract*— The low-frequency steady-state visual evoked potential (SSVEP)-based brain-computer interfaces (BCIs) tend to induce visual fatigue in the subjects. In order to enhance the comfort of SSVEP-BCIs, a novel SSVEP-BCI encoding method based on simultaneous modulation of luminance and motion is proposed. In this work, sixteen stimulus targets are simultaneously flickered and radially zoomed using a sampled sinusoidal stimulation method. The flicker frequency is set to a 30 Hz for all the targets, while assigning different radial zoom frequencies (ranging from 0.4 Hz to 3.4 Hz, with an interval of 0.2 Hz) are assigned to each target separately. Accordingly, an extended vision of the filter bank canonical correlation analysis (eFBCCA) is proposed to detect the intermodulation (IM) frequencies and classify the targets. In addition, we adopt the comfort level scale to evaluate the subjective comfort experience. By optimizing the combination of IM frequencies for the classification algorithm, the average recognition accuracy of the offline and online experiments reaches 92.74 ± 1.53% and 93.33 ± 0.01%, respectively. Most importantly, the average comfort scores are above 5. These results demonstrate the feasibility and comfort of the proposed system using IM frequencies, which provides new ideas for the further development of highly comfortable SSVEP-BCIs.**

***Index Terms*— Brain-computer interface, steady-state visual evoked potential, intermodulation frequencies, filter bank canonical correlation analysis, high frequency.**

I. Introduction

BRAIN-COMPUTER interface (BCI) is a communication pathway between human brain and external devices, which does not depend on the peripheral nerves and muscles. It provides an alternative dimension for human brain to interact with the environment [1], [2]. In clinical applications, BCI contributes in restoring and improving the physical and mental functions [3], [4], [5], [6], [7]. Due to high signal-to-noise ratio (SNR), low cost, and high availability, the steady-state visual evoked potential (SSVEP) is a widely used signal of electroencephalography (EEG) in non-invasive BCI [8], [9].

Currently, the research regarding SSVEP-BCI is focused on improving the SSVEP-BCI systems' performance and enhancing the comfort level. On one hand, the researchers have made huge efforts for building high-speed BCIs. For instance, high-speed BCIs with more than 100 targets have been continuously proposed in recent years [10], [11]. In addition, the information transfer rate (ITR) of 120-target SSVEP-BCI realized based on a spectrally dense joint frequency-phase modulation encoding method reached 213.23 ± 6.60 bits/min. Similarly, a high-speed brain speller using task-related component analysis (TRCA) that has achieved the highest ITR to date, i.e., 325.33 ± 38.17 bits/min, has been proposed [12]. On the other hand, low- and medium-frequency SSVEP stimuli, such as the stimulus frequencies below 30 Hz, are stressful for the eyes and may trigger epileptic seizures [13]. In order to reduce the visual stimulus contrast and ensure a higher level of comfort and safety, a high-frequency SSVEP stimulation method is currently being used extensively in BCI research [14], [15], [16]. However, there are some limitations of high-frequency SSVEP paradigm. The analysis regarding the subjective discomfort evaluation of SSVEP-BCI in a flicker simulation range of 5.5-86.0 Hz reveals that the subjects were unable to concentrate on the high-frequency stimulus (30 Hz to 86 Hz), as compared to the low- (5.5 Hz to 12 Hz) and mid-frequency stimuli (12.5 Hz to 29.5 Hz) [17], and SSVEP signal amplitude can be strongly influenced by attention level of subjects [18]. Interestingly, it is noteworthy that the use of flicker-free periodic motion targets for building the SSVEP-BCIs is more comfortable, causes less visual fatigue, and exhibits high performance during human-computer interaction as compared to the conventional low-frequency flicker-based paradigm [19], [20], [21], [22], [23], [24], [25]. Therefore, the superimposition of flicker-free periodic motion on top of high-frequency periodic flicker to produce two input signals with different frequencies for encoding targets can also be explored as a novel direction for further improving the comfort level of a system.

The previous studies presented in literature show that the non-linear integration of periodic input signals of different frequencies induce a frequency component other than the

Manuscript received 15 March 2023; revised 14 May 2023; accepted 26 May 2023. Date of publication 30 May 2023; date of current version 13 June 2023. This work was supported in part by the National Key Research and Development Program of China under Grant 2022YFC3602803, in part by the National Natural Science Foundation of China under Grant 62171473, and in part by the Tianjin Municipal Science and Technology Plan Project under Grant 21JCYBJC01500. *(Corresponding authors: Xiaogang Chen; Hongyan Cui.)*

This work involved human subjects or animals in its research. Approval of all ethical and experimental procedures and protocols was granted by the Institutional Review Board of Tsinghua University.

The authors are with the Institute of Biomedical Engineering, Chinese Academy of Medical Sciences and Peking Union Medical College, Tianjin 300192, China (e-mail: aamir_lemon0218@163.com; chenxg@bme.cams.cn; cuihy@bme.cams.cn).

Digital Object Identifier 10.1109/TNSRE.2023.3281416

fundamental and harmonics, known as intermodulation (IM) frequency component. In terms of value, this is equivalent to a linear combination of different input frequencies [26]. There are many ways to generate the periodic frequency of the input signal. The generation of the periodic frequency of the input signal can take many forms. Several studies use the traditional flicker frequency and other forms of periodically changing frequencies as an input signal of the evoked IM components. Giani et al. [27] demonstrated that the IM frequencies can be modulated by using the double modulation of luminance, i.e., 6 Hz, and size, i.e., 0.2 Hz, by using the red circular gratings at the visual level. Subsequently, the red circle stimulus target is also used in the study by Chen et al. [28]. The authors selected luminance modulated frequencies of 10 Hz, 12 Hz, and 15 Hz, and color modulated frequency of 0.5 Hz for encoding the eight grating targets. Afterwards, the authors proposed a novel SSVEP-based stimulation method that uses the same frequency of luminance change, i.e., 15 Hz, but different chromatic changes, i.e., red/green, to evoke the IM frequencies for encoding the nine targets [29]. The results showed that the recognition accuracies of three cases were 91.67%, 93.98%, and 96.41%, respectively. Furthermore, in order to improve the recognition of SSVEPs based on IM frequencies, the authors analyzed individual SSVEP calibration data points by using filter bank canonical correlation analysis (FBCCA) and achieved a recognition accuracy of 91.43 ± 5.52% [30]. In addition to the combination of chromatic and luminance characteristics, Pitchaimuthu et al. [31] recorded SSVEPs evoked by one luminance flicker of 6.1 Hz and two horizontal periodic motion stimuli, including 2.1 Hz and 2.4 Hz. Chi et al. [32] proposed a 2-target hybrid paradigm by combining the motor imagery and SSVEP with the hand grasp at specific frequencies, i.e., left: 1 Hz; right: 1.5 Hz. All of the above stimulation methods induced clear IM frequency components, thus demonstrating the stability of IM frequency components in target classification. There are several studies focused on introducing the motion attribute in the low-frequency SSVEP-BCIs for encoding the targets. Kwon et al. [33] demonstrated that the conventional SSVEP visual stimuli combined with appropriate periodic motion significantly increases the SSVEP amplitudes, thus improving the SSVEP-BCI performance. Yan and Xu [34] adopted five frequencies to encode nine targets and proposed a BCI method based on light-flashing and motion hybrid coding. This method evoked stable motion frequency, light-flashing frequency, its harmonic components, and weak IM components between motion and light-flashing. The average accuracy achieved by this method was 92.96%. However, please note that almost all the aforementioned methods adopt low- and medium frequencies to elicit SSVEPs. In addition, the number of targets was generally low as well, i.e., a narrow range of motion frequencies.

In this work, we present a novel stimulation method based on simultaneous modulation of luminance and motion for achieving higher comfort level for subjects. We design sixteen stimulus targets to flicker at 30 Hz and simultaneously zoom radially at different frequencies. please note that both encoding methods follow a sinusoidal function. in addition, an extended vision of FBCCA is proposed to detect IM frequency components. in order to choose the optimal experimental parameters and verify the feasibility of the proposed system, we perform offline and online experiments in this study. furthermore, we also collect the subjective comfort levels in each experiment to evaluate the comfort level of the proposed system.

II. Methods and Materials

A. Experimental Environment

1) Subjects: In the work, eighteen subjects (aged 25.3 ± 2.5 years, four males) participated in the experiments. All the subjects have normal or corrected-to-normal vision, concentration, and show no symptoms of hyperactivity or history of mental or neurological disorders. The experiments performed in this work comprise offline and online experiments. Thirteen and twelve subjects participated in the offline and online experiments, respectively. Moreover, seven participants simultaneously participated in both types of the experiments. All the participants completed the consent form and are informed about the whole experimental procedure before the onset. Additionally, all the participants are paid at the end of the experiment. The Institutional Review Board of Tsinghua University approved the grant for conducting this study.

2) Experiment Equipment and Data Acquisition: The scalp EEG data are recorded by using the Synamps2 system developed by Neuroscan at a sample rate of 1000 Hz and then trapped at 50 Hz for removing the interference caused by the industrial frequencies. The international 10-20 modified 64-channel EEG scalp is adopted to acquire the EEG data. In the offline experiments, the data acquisition is performed with 60 channels, expected M1, M2, CB1, and CB2, with the reference electrode at the left posterior mastoid. In the online experiments, only 9 channels are used for performing data acquisition, including Pz, Oz, O1, O2, POz, PO3, PO4, PO5, and PO6. In both experiments, the ground electrode is located at the midpoint of Fz and FPz and all the electrode impedances are below 10 kΩ. In addition, the recorded EEG signals are sent to the stimulus device via TCP/IP protocol for performing real-time feedback analysis. The user interaction interface is realized using the Psychtoolbox of MATLAB.

B. Experimental Design

1) Paradigm Design: In both offline and online experiments, the user interaction interface is displayed on a 1920 × 1080-pixel LCD monitor with a refresh rate of 120 Hz. Based on the previous comparative experiments, the performance of green or circle stimulus paradigm is more stable [35], [36] and the luminance contract ratio (LCR) of green-black paradigm is lower [37]. The stimulus presentation interface is presented in Fig. 1(a), where 16 green circles (the RGB value is 0, 255, 0) of 200 × 200 pixels distribute in a 4 × 4 layout, and the number from 1 to 16 locate in the center of each circle target. Additionally, the horizontal and vertical distance between the targets is 280 pixels and 70 pixels, respectively. The horizontal and vertical margins are 140 pixels and 35 pixels, respectively.

In this work, the periodic changes in luminance and size are realized based on sinusoidal sampling encoding method.

Specifically, the stimulus sequence of luminance changes is mathematically expressed as follows:

$$s\,(F,i) = \frac{1}{2} \times \{1 + sin[2\pi F(i/R)]\} \tag{1}$$

where, F denotes the flicker frequency. In this work, the value of F is set to 30 Hz for all 16 targets. i denotes the frame index in a stimulus sequence and R represents the screen refresh rate. The dynamic range of stimulus sequence $s\,(F,i)$, ranges from 0 to 1, where 0 and 1 indicate the minimum and maximum luminance, respectively.

Fig. 1(b) presents the changes in the size of one stimulus. The radial variation sequences are mathematically expressed as follows:

$$r\,(f_k,i) = Asin[2\pi F(i/R)] - A, \quad k = 1,2,\ldots,16 \tag{2}$$

where, k denotes the serial number of stimulus targets, f_k denotes the radial zoom frequencies ranging from 0.2 - 3.4 Hz with an interval of 0.2 Hz, and A denotes the radius of the radial zoom with a value of 40 pixels.

2) Experiment Procedure: In this work, we perform offline and online experiments. Before starting the experiments, the subjects are asked to sit in a chair 90 cm away from a monitor and remain relaxed.

The offline experiments consist of 10 blocks, and each block consists of 16 trails. Each trail starts with a red circle being displayed for 0.5 s to cue the next stimulus target. Please note that the location and the size of the red circle is same as the stimulus target to be presented. Then, all stimulus targets start flickering at the same frequency and zoom radially at different frequencies simultaneously. The task duration is set to 5 s. Subsequently, all the targets stop flickering and zooming during the 0.5 s interval, and the size of the stimulus targets is restored to the initial state. A rest period is allowed between each block depending on the fatigue level of the subjects. In addition, all the subjects are asked to rate the comfort level after the experiments.

The online experiments are performed to verify the feasibility and stability of this paradigm by using the optimized data length. This optimized length is obtained by analyzing the results of the offline experiments. Similar to offline experiments, in online experiments, there are 10 blocks in one experiment as well. Each block consists of 16 trails. Each trial contains 0.5-s prompt time and 4-s task time. Therefore, the proposed system outputs a command every 4.5 s. The cue for the next target appears right after the stimulus offset. The subjects receive real-time auditory feedback in the form of a beep when the recognition result matches the cue target.

According to [38], the comfort level scale is completed after the offline and online experiments by each subject. The subjects are asked to score the comfort level based on a 6-point scale ranging from 1 (totally unacceptable) to 6 (a good experience).

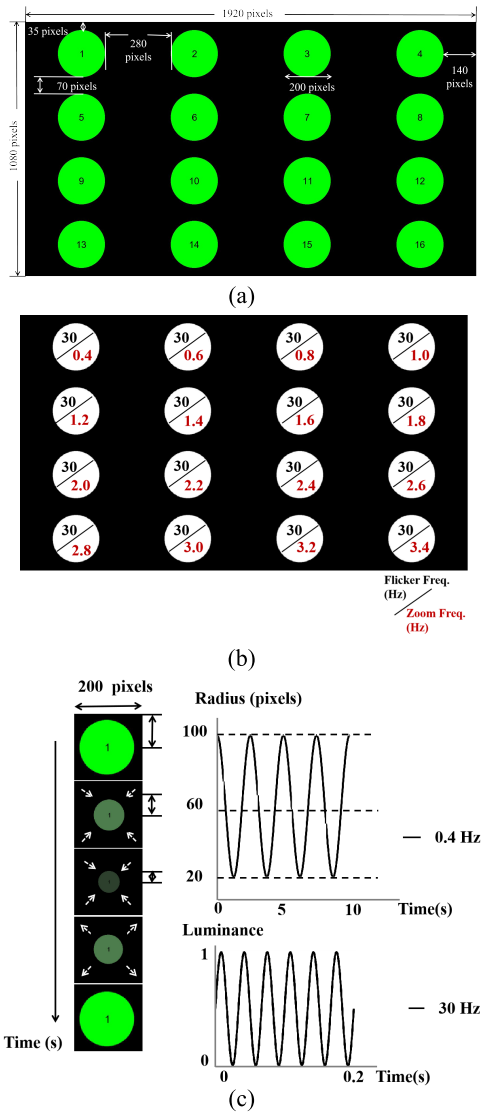

Fig. 1. Experimental paradigm design. (a) Layout of the 16 targets on screen. (b) The flicker frequency and radial zoom frequency of each target. (c) Stimulus encoding method based on simultaneous modulation of luminance and motion (motion modulation in 0.4Hz for example).

C. Signal Processing

1) FFT: The fast Fourier transform (FFT) in the time domain is adopted to calculate the SSVEP amplitude spectrum in all the trails. The EEG data used in this work are averaged over all the subjects obtained at the Oz channel with a data length of 5 s in the offline experiments.

2) FBCCA: FBCCA is an untrained algorithm for performing EEG signal analysis [39]. Originally, the FBCCA method exploited different spectral characteristics of the fundamental and harmonic components of SSVEPs. First, multiple sub-band signals ($X_{SB_n}, n = 1,2,\ldots,N$) are extracted by zero-phase Chebyshev type I infinite impulse response (IIR) filters from original EEG signals X. The filtfilt function in MATLAB is used to meet the zero-phase requirement. Second, the standard canonical correlation analysis is performed to calculate the correlation vector ρ_k between each sub-band component ($X_{SB_n}, n = 1,2,\ldots,N$) and the reference signals ($Y_{f_k}, k = 1,2,\ldots,16$) corresponding to all the stimulus

frequencies f_k. The reference signals are set to:

$$Y_f = \begin{bmatrix} sin\,(2\pi f t) \\ cos\,(2\pi f t) \\ \vdots \\ sin\,(2\pi N_h f t) \\ cos\,(2\pi N_h f t) \end{bmatrix}, \quad t = \left[\frac{1}{f_s}, \ldots, \frac{N_p}{f_s}\right] \tag{3}$$

where, N_h denotes the number of harmonics, N_p denotes the number of sampling points, and f_s denotes the sampling frequency. The correlation vector ρ_k is defined as follows:

$$\rho_k = \begin{bmatrix} \rho_k^1 \\ \rho_k^2 \\ \vdots \\ \rho_k^N \end{bmatrix} = \begin{bmatrix} \rho(X_{SB_1}^T W_X \left(X_{SB_1} Y_{f_k}\right), Y^T W_Y \left(X_{SB_1} Y_{f_k}\right)) \\ \rho(X_{SB_2}^T W_X \left(X_{SB_2} Y_{f_k}\right), Y^T W_Y (X_{SB_2} Y_{f_k})) \\ \vdots \\ \rho(X_{SB_N}^T W_X \left(X_{SB_N} Y_{f_k}\right), Y^T W_Y (X_{SB_N} Y_{f_k})) \end{bmatrix} \tag{4}$$

where, $\rho\,(x, y)$ represents the correlation coefficient of x and y and k represents the number of visual stimulus targets. Finally, the feature $\tilde{\rho}$ used for target identification is calculated as the weighted sum of the squares of the correlation values corresponding to each sub-band signal.

$$\tilde{\rho}_k = \sum_{i=1}^{N} w(i) \cdot \left(\rho_k^i\right)^2 \tag{5}$$

The frequency of the reference signal corresponding to the maximum correlation coefficient is then considered to be the frequency of SSVEPs.

$$f_{target} = \max_{f_k} \tilde{\rho}_k \tag{6}$$

3) Extended-FBCCA: In this work, an extended version of FBCCA (eFBCCA) is proposed to utilize the information in the IM frequency components elicited by the interaction of periodic luminance changes and radial motion changes. In case of eFBCCA, the reference signal is designed to include the IM frequency components as follows:

$$Y_{f_k} = \begin{bmatrix} sin\left(2\pi(F - f_k)t\right) \\ cos\left(2\pi(F - f_k)t\right) \\ sin\left(2\pi(F + f_k)t\right) \\ cos\left(2\pi(F + f_k)t\right) \\ \vdots \\ sin\left(2\pi(N_h{*}F - N_{IM} * f_k)t\right) \\ cos\left(2\pi(N_h{*}F - N_{IM} * f_k)t\right) \\ sin\left(2\pi(N_h{*}F + N_{IM} * f_k)t\right) \\ cos\left(2\pi(N_h{*}F + N_{IM} * f_k)t\right) \end{bmatrix}, \quad t = \left[\frac{1}{f_s}, \ldots, \frac{N_p}{f_s}\right] \tag{7}$$

where, F denotes the flicker frequency and f_k represents the radial zoom frequency. In this work, N_h is set to 2. N_{IM} denotes the number of IM component harmonics.

In addition, the weights $w(i)$ of the sub-bands in (5) are defined as follows:

$$w(i) = i^{-a} + b, \quad i = 1, 2 \tag{8}$$

where, i denotes the number of sub-bands and is set to 2 in this work. a and b represent the constants that are set to 1.25 and 0.25, respectively, based on a previous study [38].

D. System Performance Evaluation

The ITR is an important metric for assessing the performance of SSVEP-BCIs in addition to the recognition accuracy. The ITR is mathematically expressed as follows:

$$ITR = \left(log_2 N + P * log_2 P + (1 - P) * log_2 \frac{1 - P}{N - 1}\right) * \left(\frac{60}{T}\right) \tag{9}$$

where, N represents the number of visual stimulus targets, P denotes the recognition accuracy rate, and T represents the time required to issue a single command, which included the gaze-shifting time of 0.5 s.

III. Results

A. Offline Experiment Results

Based on previous studies that investigate the IM components [28], [29], the average EEG data of 5-s duration recorded in the Oz channel of all subjects is used to draw the SSVEP spectrum of all targets, as presented in Fig. 2. Please note that there are significant peaks at both the fundamental frequency and the second harmonics of all the targets. In addition, the IM frequency components of varying number and amplitude generated by the interaction of changes in the luminance frequencies and size frequencies, also appear for all the targets. The number of IM harmonics with significant peaks resulting from the IM of luminance changes and motion changes is at most two for all the targets. Specifically, there are $F \pm f$ and $2F \pm f$ IM components for 0.4 Hz and 0.6 Hz zoom frequency conditions. For zoom frequency conditions from 0.8 to 1.8 Hz, the IM components including, $F \pm f$, $F \pm 2f$, $2F \pm f$, $2F \pm 2f$ appear to varying degrees. However, the absence of $F - f$ occurs for zoom frequencies, which are greater than 2 Hz. In summary, only $F + f$ IM components appear in all the targets. Therefore, one-way repeated measures ANOVA shows that there is no significant difference between the amplitudes of the $F + f$ IM components for all the targets ($p > 0.05$).

The SSVEP amplitude topographies of $F + f$ IM components of all the targets are plotted in Fig. 3. The topographies of the $F + f$ IM component SSVEP signals elicited by the 16 different zoom frequencies are similar, and the strong SSVEPs are mainly obtained in the parieto-occipital area, especially at the Oz electrode channel.

Given the difference in IM frequency components across the 16 targets, different combinations of IM components (see Table I are used in the construction of the reference signal template to select the combination with the best classification performance [40].

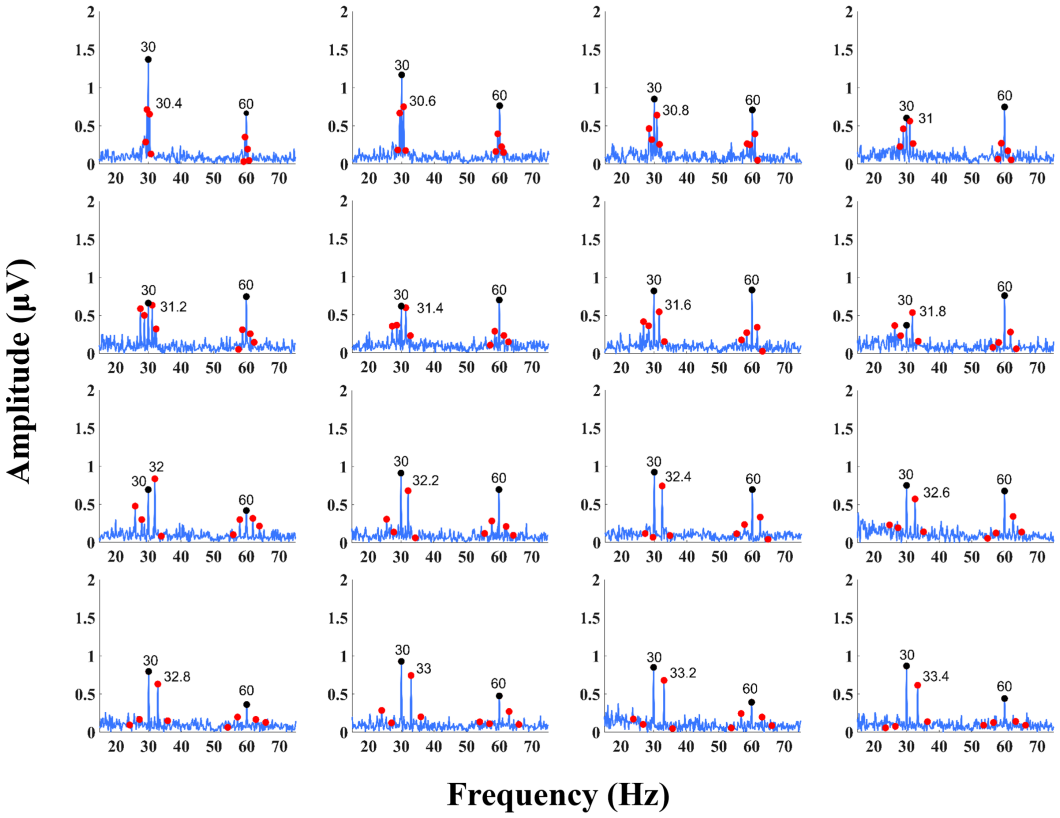

Fig. 2. SSVEP amplitudes of the averaged EEG signals of all the subjects at the Oz channel for all 16 radial zoom frequencies. Black circles indicate the fundamental frequency (i.e., 30 Hz) and second harmonics, and red circles represent the IM components. Red circles indicate the IM frequency components, and black circles represent the fundamental and harmonic frequencies of luminance changing. The layout of the 16 SSVEP amplitude subplots corresponds to the target order of the stimulus interface.

TABLE I
COMBINATIONS OF IM FREQUENCY COMPONENTS USED IN THE REFERENCE SIGNAL

Combinations	Types of IM components
CB1	$F+f$
CB2	$F \pm f$
CB3	$F \pm f,\quad F \pm 2f$
CB4	$F \pm f,\quad 2F \pm f$
CB5	$F \pm f,\quad F \pm 2f,\quad 2F \pm f$
CB6	$F \pm f,\quad F \pm 2f,\quad 2F \pm f,\ 2F \pm 2f$

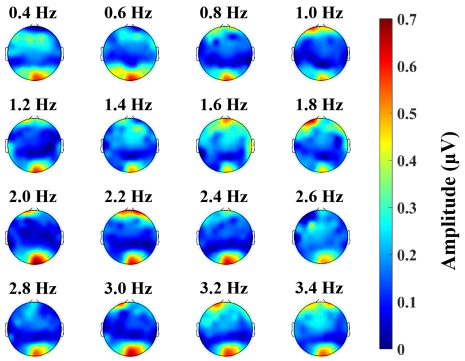

Fig. 3. Average $F+f$ IM frequency SSVEP amplitude topographies of all subjects at Oz channel.

Therefore, the recognition accuracies corresponding to the six combination of IM components are calculated for all 13 subjects, as presented in Table II. The recognition accuracy of the condition of CB5 achieves 92.89 ± 1.54%, which is adopted for eFBCCA. According to a one-way repeated measure ANOVA, different combinations have a significant influence on the recognition accuracy ($p < 0.05$), and a significant difference level is marked, as presented in Fig. 4, where CB5 is significantly different from all other conditions except CB3.

Fig. 5 shows the recognition accuracy and ITR performance of the system for data samples of different lengths. It is evident that the average recognition accuracy increases with an increase in the data length and reaches its highest value (92.74 ± 0.02%) at the data length of 5 s. The ITR peaks (41.27 ± 3.09 bits/min) when the data length is 3.5 s. Generally, a data length of 3.5 s is chosen to build the online experiments. Nevertheless, a paired t-test shows that there exists a significant difference between the recognition accuracy corresponding to 3.5 s and 4 s data length ($p < 0.05$). Finally, in order to balance the ITR and a higher recognition accuracy, a data length of 4 s is selected as the task time in online experiments. This selection is done based on a paired t-test, which shows that there is no difference between the ITR value obtained with 3.5 s and 4 s data length ($p > 0.05$). The recognition accuracy and ITR at 4 s data length are 86.88 ± 0.03% and 39.95 ± 2.54 bits/min, respectively.

Fig. 6 shows the average recognition accuracies of thirteen subjects for 16 radial zoom frequencies in the form of

TABLE II
RESULTS OF THE OFFLINE EXPERIMENTS TESTING 13 SUBJECTS FOR DIFFERENT COMBINATIONS

Subjects	Accuracy (%)					
	CB1	CB2	CB3	CB4	CB5	CB6
S1	81.25	88.12	95.00	81.87	92.5	89.37
S2	100	98.12	100	99.38	100	100
S3	96.88	98.75	97.50	95.63	99.38	98.13
S4	90.63	90.00	87.50	94.37	96.88	93.13
S5	58.13	72.50	80.63	80.63	87.50	88.13
S6	65.00	70.00	81.87	78.13	86.88	78.75
S7	92.5	88.12	96.13	93.13	93.13	86.25
S8	77.50	78.75	91.25	83.75	95.00	92.50
S9	43.13	71.25	72.50	84.38	90.00	86.25
S10	100	100	96.88	100	100	95.00
S11	96.88	97.50	91.25	98.12	96.25	88.13
S12	40.63	65.00	71.88	71.25	80.63	78.75
S13	29.38	35.00	52.50	86.88	87.50	82.50
Average ± SE	74.76 ± 6.40	81.01 ± 4.74	85.5 ± 3.46	88.27 ± 2.35	92.74 ± 1.53	88.99 ± 1.72

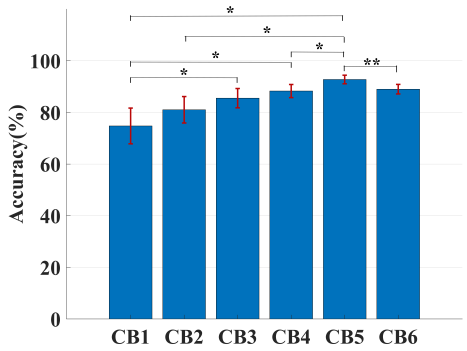

Fig. 4. Average recognition accuracy of six combinations of the offline experiment for 13 subjects with error bar and significance marks (*$p < 0.05$, **$p < 0.01$). The error bars indicate the standard error (SE).

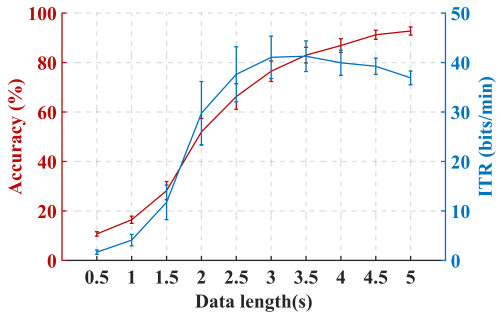

Fig. 5. System performance with different data lengths. The error bars indicate the standard error (SE).

a confusion matrix and histogram. As shown in Fig. 6(a), the average recognition accuracies of all the targets are greater than 83% and the highest recognition accuracy reaches 97.69%. In Fig. 6(b), one-way repeated measures ANOVA is used for obtaining the recognition accuracy corresponding to different zoom frequencies. Please note that there exists no significant difference between 16 different zoom frequency conditions (for all conditions $p > 0.05$). In conclusion, all 16 targets of the system are accurately identified.

B. Online Experiment Results

Based on parameters optimized of offline experiments, a 4-s stimulation duration was chosen for building the online validation experiments. In addition, each trail contained 0.5-s gaze-shifting time. Thus, the output of the online system is 4.5 s. The BCI performance recorded in the online experiments is shown in Table III. The average recognition accuracy and ITR of all subjects are 93.33 ± 0.01% and 45.47 ± 1.33 bits/min, respectively. The recognition accuracy is above that of the offline experiments and are both above 90%, validating the feasibility and stability of the proposed novel stimulus encoding method based on simultaneous modulation of luminance and motion using IM frequencies. Since seven subjects participated in both offline and online experiments, a paired t-test is performed to show that the classification performance between offline and online experiments is comparable ($p > 0.05$), which provides robust evidence for the stability of the system. In addition, the average recognition accuracy of the five subjects who did not participate in the offline experiments was also over 90%, further demonstrating the usability of the proposed system.

C. Comfort Level and Anti-Fatigue Performance Assessment

Based on the work presented in [35], in order to evaluate the anti-fatigue performance of the proposed system, the comparison of the average recognition accuracy of the first five blocks and the last five blocks of the offline experiment for all 13 subjects is presented in Fig. 7. The average recognition accuracies of all the subjects in level 1 and level 2 are 92.40 ±

TABLE III
RESULTS OF THE ONLINE EXPERIMENTS TESTING 12 SUBJECTS

Subjects	Accuracy (%)	ITR (bits/min)
S1*	95.00	46.91
S2*	98.75	51.39
S3*	97.50	49.78
S4*	93.13	44.94
S5*	91.25	43.07
S7*	89.38	41.29
S11*	98.12	50.57
S14	94.38	46.24
S15	86.25	38.47
S16	96.88	37.93
S17	95.63	47.60
S18	83.75	36.33
Average ± SE	93.33 ± 0.01	45.47 ± 1.33

The subjects number marked with '*' were those who also took part in the offline experiment.

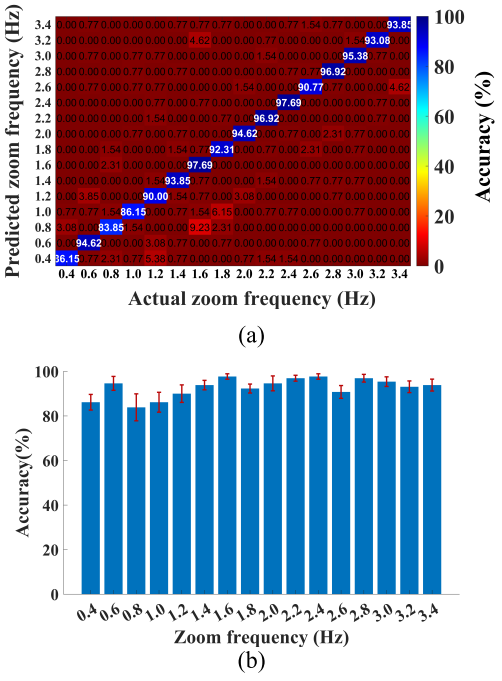

Fig. 6. The average recognition accuracies of all subjects for 16 radial zoom frequencies at 5 s data length display as a confusion matrix (a) and histogram (b). The error bars indicate the standard error (SE).

1.90% and 93.08 ± 2.26%, respectively. The paired samples t-test shows that there is no significant difference between two levels, indicating that the proposed paradigm has good anti-fatigue performance.

Fig. 8 shows the comfort scores of all the subjects, each in the form of a histogram. The mean score of comfort level scale is 5.23 ± 0.18 in the offline experiments and 5.50 ± 0.19 in the online experiments, respectively. These results indicate that the subjects were able to perform this experimental task in a comfortable state. Furthermore, the

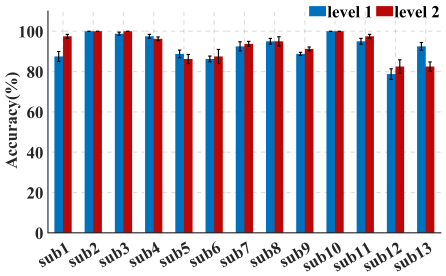

Fig. 7. Comparison of the average recognition accuracy of two levels of the offline experiment for all 13 subjects. The error bars indicate the standard error (SE). (Level 1: the first five blocks, level 2: the last five blocks).

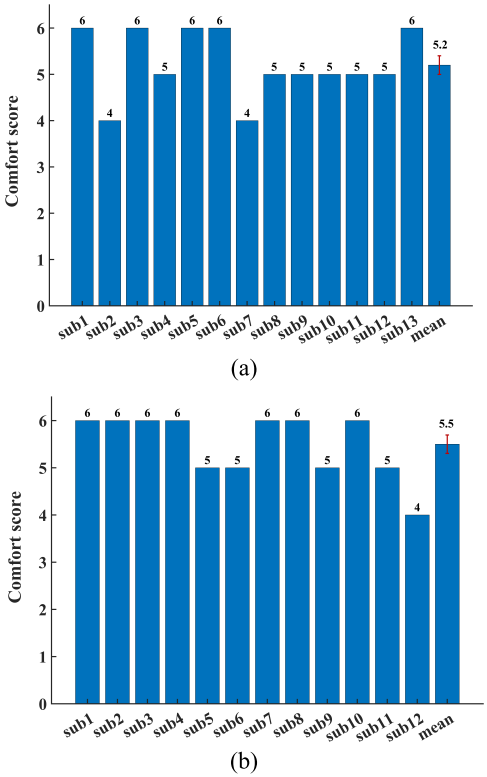

Fig. 8. The comfort scores and its average value of all subjects in offline experiments (a) and online experiments (b). The error bars indicate the standard error (SE).

paired t-test confirms that there is no significant difference between the subjective comfort ratings of the system in the offline and online experiments of seven subjects ($p > 0.05$). Therefore, this analysis further demonstrates the stability and high comfort level of the proposed system.

IV. DISCUSSION

In this work, a novel stimulus encoding method based on the simultaneous modulation of luminance and motion using IM frequencies is proposed for comfortable visual experience. After using the offline experiments to select the best parameters and online experiments to validate the proposed novel paradigm, it is evident that the proposed paradigm improves the subjective comfort of the subjects while ensuring the accuracy of target recognition.

The simultaneous modulation of luminance and motion encoding method designed in this work elicit significant IM frequency components, which is similar with the results of

previous studies [31], [34]. Specifically, the stimulus target designed by Yan and Xu [34] is presented as a circle with a rotating motion in the center and a periodic light-flashing around the periphery of the circle. The frequencies of light-flashing are below 12 Hz. As the performance of high-frequency SSVEP-BCIs has improved steadily in recent years, their usability has increased as compared to the low-frequency SSVEP-BCIs. However, there is a gap in research regarding the combination of high-frequency SSVEP and FF-SSMVEP as far as we know based on our investigation. Therefore, this work innovatively combines high-frequency flicker with radial zoom to encode the same area of the stimulus target. The interaction between these two factors successfully induces distinct IM components. In addition, we further increase the number of encoding targets for the novel system to sixteen. It is noteworthy that the number of encoding targets is an important metric used to assess the performance of paradigms. Therefore, this improvement is meaningful for future works on the design of SSMVEP-based BCIs. Moreover, the paradigm can be used more effectively to assess the anti-fatigue performance of a system as the task duration becomes longer and the number of encoding targets increases. For future research, we intend to construct a static paradigm to compare with the motion paradigm for verification to increase the power of the conclusions. In addition to the innovations in the design of experimental paradigms, we also made some adjustments in the traditional algorithm. The FBCCA has been widely used as an untrained algorithm for detecting SSVEPs [39], [41], and some improvements have been made in several studies [42], [43]. In this work, an extended version of the traditional FBCCA is proposed to detect the IM frequencies and reach the recognition accuracy of over 90% in both offline and online experiments. In addition, we calculated the recognition accuracy performance of the system using the eCCA method, which were 87.88 % and 84.74 % in the offline and online experiments, respectively. These results were lower than the system performance obtained using the proposed eFBCCA method, demonstrating that the proposed eFBCCA method superior to the eCCA method. Furthermore, trained algorithms are considered to evaluate the performance of the system in future studies. For example, the average recognition accuracies obtained by the TDCA [44] trained algorithm were 97.65% and 98.47%, respectively, at the data length of 5 s in the offline experiment and 4 s in the online experiments, which is more beneficial to improve the practicality and robustness of the system. Lastly, the subjective evaluation of the mean comfort level score above 5 also validates the conclusion of previous studies [35], [36], [37], i.e., the green-circle-zoom stimulus paradigm performs effectively in improving the subjective comfort of the subjects.

Further investigation of the modulation of high-frequency luminance changes and motion can be explored in three directions. First, by increasing the number of encoding targets. The relatively high frequency range of the SSVEP response is limited. Therefore, increasing the number of targets reduces the frequency resolution, which in turn makes classification more difficult [13]. The previous studies show that the hybrid paradigm has a great potential for increasing the number of targets [27], [45]. In this work, only one flicker frequency is used for pilot study in order to verify whether the different radial zoom frequencies can be intermodulated with the high-frequency flickering property. The results show that it is possible to set different high frequencies of luminance change with motion property if the expansion target is considered. Second, developing more comfortable BCIs and introducing them into practical applications. In this work, only one flicker frequency and 16 radial zoom frequencies are explored for the preliminary experiments. Subsequently, we can focus on exploring a wider range of frequencies to see if the comfort level can be further improved. Furthermore, Ravi et al. [46] proved that the SSMVEP stimulus is more robust to the changes in the background as compared to the SSVEP stimulus in AR. Notably, the proposed paradigm has a potential to enhance the user comfort in this scene. Additionally, it also provides new ideas for a better visual experience for users in daily entertainment or clinical rehabilitation. Finally, in addition to the commonly used algorithms for decoding SSVEPs, we intend to introduce advanced machine learning algorithms [47], [48], [49], [50] into the identification and decoding of intermodulation frequency components to achieve better system performance.

V. Conclusion

We adopted sampled sinusoidal stimulation method to build a 16-target paradigm in which the stimulus targets were simultaneously encoded with the same flicker frequency and a range of radial scaling frequencies. Based on the use of an optimized combination of IM frequencies in offline and online experiments, the average recognition accuracy reached 92.74 $\pm$ 1.53 % and 93.33 $\pm$ 0.01 %, respectively. Most importantly, the average comfort scores were both above 5. These results demonstrate the feasibility and comfort of the proposed system using IM frequencies. In summary, the proposed novel stimulus encoding method provides an alternative solution for conventional SSVEP-BCIs and expands the horizon for the further development of exceptionally comfortable SSVEP-BCIs.

References

[1] J. R. Wolpaw et al., "Brain-computer interface technology: A review of the first international meeting," *IEEE Trans. Rehabil. Eng.*, vol. 8, no. 2, pp. 164–173, Jun. 2000.

[2] M. F. Mridha, S. C. Das, M. M. Kabir, A. A. Lima, M. R. Islam, and Y. Watanobe, "Brain-computer interface: Advancement and challenges," *Sensors*, vol. 21, no. 17, p. 5746, Aug. 2021.

[3] S. Luo, Q. Rabbani, and N. E. Crone, "Brain-computer interface: Applications to speech decoding and synthesis to augment communication," *Neurotherapeutics*, vol. 19, no. 1, pp. 263–273, Jan. 2022.

[4] A. Colucci et al., "Brain–computer interface-controlled exoskeletons in clinical neurorehabilitation: Ready or not?" *Neurorehabil. Neural Repair*, vol. 36, no. 12, pp. 747–756, Dec. 2022.

[5] K. Värbu, N. Muhammad, and Y. Muhammad, "Past, present, and future of EEG-based BCI applications," *Sensors*, vol. 22, no. 9, p. 3331, Apr. 2022.

[6] U. Chaudhary, N. Birbaumer, and A. Ramos-Murguialday, "Brain-computer interfaces for communication and rehabilitation," *Nature Rev. Neurol.*, vol. 12, no. 9, pp. 513–525, Sep. 2016.

[7] L. Chen et al., "Adaptive asynchronous control system of robotic arm based on augmented reality-assisted brain–computer interface," *J. Neural Eng.*, vol. 18, no. 6, Nov. 2021, Art. no. 066005.

[8] Y. Wang, X. Gao, B. Hong, C. Jia, and S. Gao, "Brain-computer interfaces based on visual evoked potentials," *IEEE Eng. Med. Biol. Mag.*, vol. 27, no. 5, pp. 64–71, Sep. 2008.

[9] S. Gao, Y. Wang, X. Gao, and B. Hong, "Visual and auditory brain-computer interfaces," *IEEE Trans. Biomed. Eng.*, vol. 61, no. 5, pp. 1436–1447, May 2014.

[10] Y. Chen, C. Yang, X. Ye, X. Chen, Y. Wang, and X. Gao, "Implementing a calibration-free SSVEP-based BCI system with 160 targets," *J. Neural Eng.*, vol. 30, no. 4, Jul. 2021, Art. no. 046094.

[11] X. Chen, B. Liu, Y. Wang, and X. Gao, "A spectrally-dense encoding method for designing a high-speed SSVEP-BCI with 120 stimuli," *IEEE Trans. Neural Syst. Rehabil. Eng.*, vol. 30, pp. 2764–2772, 2022.

[12] M. Nakanishi, Y. Wang, X. Chen, Y. Wang, X. Gao, and T. Jung, "Enhancing detection of SSVEPs for a high-speed brain speller using task-related component analysis," *IEEE Trans. Biomed. Eng.*, vol. 65, no. 1, pp. 104–112, Jan. 2018.

[13] D. Zhu, J. Bieger, G. G. Molina, and R. M. Aarts, "A survey of stimulation methods used in SSVEP-based BCIs," *Comput. Intell. Neurosci.*, vol. 2010, Jan. 2010, Art. no. 702357.

[14] L. Liang, C. Yang, Y. Wang, and X. Gao, "High-frequency SSVEP stimulation paradigm based on dual frequency modulation," in *Proc. 41st Annu. Int. Conf. IEEE Eng. Med. Biol. Soc. (EMBC)*, Jul. 2019, pp. 6184–6187.

[15] S. Ladouce, L. Darmet, J. J. Torre Tresols, S. Velut, G. Ferraro, and F. Dehais, "Improving user experience of SSVEP BCI through low amplitude depth and high frequency stimuli design," *Sci. Rep.*, vol. 12, no. 1, p. 8865, May 2022.

[16] X. Chen, B. Zhao, Y. Wang, and X. Gao, "Combination of high-frequency SSVEP-based BCI and computer vision for controlling a robotic arm," *J. Neural Eng.*, vol. 16, no. 2, Apr. 2019, Art. no. 026012.

[17] G. S. Ferreira, P. F. Diez, and S. M. T. Müller, "Analysis about SSVEP response to 5.5–86.0 Hz flicker stimulation," in *Proc. XXVII Brazilian Congr. Biomed. Eng. (CBEB)*, in IFMBE Proceedings, vol. 83, T. F. Bastos-Filho, E. M. de Oliveira Caldeira, and A. Frizera-Neto, Eds., 2020, pp. 1581–1587.

[18] M. M. Müller, P. Malinowski, T. Gruber, and S. A. Hillyard, "Sustained division of the attentional spotlight," *Nature*, vol. 424, no. 6946, pp. 309–312, Jul. 2003.

[19] J. Xie, G. Xu, J. Wang, M. Li, C. Han, and Y. Jia, "Effects of mental load and fatigue on steady-state evoked potential based brain computer interface tasks: A comparison of periodic flickering and motion-reversal based visual attention," *PLoS ONE*, vol. 11, no. 9, Sep. 2016, Art. no. e0163426.

[20] X. Chai, Z. Zhang, K. Guan, G. Liu, and H. Niu, "A radial zoom motion-based paradigm for steady state motion visual evoked potentials," *Frontiers Hum. Neurosci.*, vol. 13, pp. 127–309, Apr. 2019.

[21] E. Perez-Valero, M. A. Lopez-Gordo, and M. A. Vaquero-Blasco, "An attention-driven videogame based on steady-state motion visual evoked potentials," *Expert Syst.*, vol. 38, no. 4, Jun. 2021, Art. no. e12682.

[22] Y. Gao, A. Ravi, and N. Jiang, "Effect of competing stimuli for steady-state visually evoked potential and steady-state motion visually evoked potential," *IEEE Access*, vol. 9, pp. 129820–129829, 2021.

[23] W. Yan, G. Xu, J. Xie, M. Li, and Z. Dan, "Four novel motion paradigms based on steady-state motion visual evoked potential," *IEEE Trans. Biomed. Eng.*, vol. 65, no. 8, pp. 1696–1704, Aug. 2018.

[24] P. Stawicki and I. Volosyak, "Comparison of modern highly interactive flicker-free steady state motion visual evoked potentials for practical brain–computer interfaces," *Brain Sci.*, vol. 10, no. 10, p. 686, Sep. 2020.

[25] C. Han, G. Xu, J. Xie, C. Chen, and S. Zhang, "Highly interactive brain–computer interface based on flicker-free steady-state motion visual evoked potential," *Sci. Rep.*, vol. 8, no. 1, p. 5835, Apr. 2018.

[26] N. Gordon, J. Hohwy, M. J. Davidson, J. J. A. van Boxtel, and N. Tsuchiya, "From intermodulation components to visual perception and cognition—A review," *NeuroImage*, vol. 199, pp. 480–494, Oct. 2019.

[27] A. S. Giani, E. Ortiz, P. Belardinelli, M. Kleiner, H. Preissl, and U. Noppeney, "Steady-state responses in MEG demonstrate information integration within but not across the auditory and visual senses," *NeuroImage*, vol. 60, no. 2, pp. 1478–1489, Apr. 2012.

[28] X. Chen, Z. Chen, S. Gao, and X. Gao, "Brain–computer interface based on intermodulation frequency," *J. Neural Eng.*, vol. 10, no. 6, Dec. 2013, Art. no. 066009.

[29] X. Chen, Y. Wang, S. Zhang, S. Gao, Y. Hu, and X. Gao, "A novel stimulation method for multi-class SSVEP-BCI using intermodulation frequencies," *J. Neural Eng.*, vol. 14, no. 2, Apr. 2017, Art. no. 026013.

[30] X. Chen, Y. Wang, S. Zhang, and X. Gao, "Enhancing detection of SSVEPs with intermodulation frequencies using individual calibration data," in *Proc. Annu. Int. Conf. IEEE Eng. Med. Biol. Soc.*, Jul. 2018, pp. 2531–2534.

[31] K. Pitchaimuthu et al., "Steady state evoked potentials indicate changes in nonlinear neural mechanisms of vision in sight recovery individuals," *Cortex*, vol. 144, pp. 15–28, Nov. 2021.

[32] X. Chi, C. Wan, C. Wang, Y. Zhang, X. Chen, and H. Cui, "A novel hybrid brain-computer interface combining motor imagery and intermodulation steady-state visual evoked potential," *IEEE Trans. Neural Syst. Rehabil. Eng.*, vol. 30, pp. 1525–1535, 2022.

[33] J. Kwon, J. Hwang, H. Nam, and C.-H. Im, "Novel hybrid visual stimuli incorporating periodic motions into conventional flickering or pattern-reversal visual stimuli for steady-state visual evoked potential-based brain-computer interfaces," *Frontiers Neuroinform.*, vol. 16, Sep. 2022, Art. no. 997068.

[34] W. Yan and G. Xu, "Brain–computer interface method based on light-flashing and motion hybrid coding," *Cogn. Neurodyn.*, vol. 14, no. 5, pp. 697–708, Oct. 2020.

[35] X. Chai, Z. Zhang, K. Guan, T. Zhang, J. Xu, and H. Niu, "Effects of fatigue on steady state motion visual evoked potentials: Optimised stimulus parameters for a zoom motion-based brain-computer interface," *Comput. Methods Programs Biomed.*, vol. 196, Nov. 2020, Art. no. 105650.

[36] A. Duszyk et al., "Towards an optimization of stimulus parameters for brain-computer interfaces based on steady state visual evoked potentials," *PLoS ONE*, vol. 9, no. 11, Nov. 2014, Art. no. e112099.

[37] R. Karimi, A. Mohammadi, A. Asif, and H. Benali, "DF-SSmVEP: Dual frequency aggregated steady-state motion visual evoked potential design with bifold canonical correlation analysis," *Sensors*, vol. 22, no. 7, p. 2568, Mar. 2022.

[38] X. Zhao, Z. Wang, M. Zhang, and H. Hu, "A comfortable steady state visual evoked potential stimulation paradigm using peripheral vision," *J. Neural Eng.*, vol. 18, no. 5, Apr. 2021, Art. no. 056021.

[39] X. Chen, Y. Wang, S. Gao, T.-P. Jung, and X. Gao, "Filter bank canonical correlation analysis for implementing a high-speed SSVEP-based brain–computer interface," *J. Neural Eng.*, vol. 12, no. 4, Aug. 2015, Art. no. 046008.

[40] X. Zhang, G. Xu, A. Ravi, S. Pearce, and N. Jiang, "Can a highly accurate multi-class SSMVEP BCI induce sensory-motor rhythm in the sensorimotor area?" *J. Neural Eng.*, vol. 18, no. 3, Mar. 2021, Art. no. 035001.

[41] X. Chen, B. Zhao, Y. Wang, S. Xu, and X. Gao, "Control of a 7-DOF robotic arm system with an SSVEP-based BCI," *Int. J. Neural Syst.*, vol. 28, no. 8, Oct. 2018, Art. no. 1850018.

[42] Y. Chen, C. Yang, X. Chen, Y. Wang, and X. Gao, "A novel training-free recognition method for SSVEP-based BCIs using dynamic window strategy," *J. Neural Eng.*, vol. 18, no. 3, Mar. 2021, Art. no. 036007.

[43] S. Ge, Y. Jiang, P. Wang, H. Wang, and W. Zheng, "Training -free steady-state visual evoked potential brain–computer interface based on filter bank canonical correlation analysis and spatiotemporal beamforming decoding," *IEEE Trans. Neural Syst. Rehabil. Eng.*, vol. 27, no. 9, pp. 1714–1723, Sep. 2019.

[44] B. Liu, X. Chen, N. Shi, Y. Wang, S. Gao, and X. Gao, "Improving the performance of individually calibrated SSVEP-BCI by task-discriminant component analysis," *IEEE Trans. Neural Syst. Rehabil. Eng.*, vol. 29, pp. 1998–2007, 2021.

[45] W. Yan and G. Xu, "A novel motion coupling coding method for brain-computer interfaces," *Biomed. Eng.*, vol. 65, no. 5, pp. 531–541, Oct. 2020.

[46] A. Ravi, J. Lu, S. Pearce, and N. Jiang, "Enhanced system robustness of asynchronous BCI in augmented reality using steady-state motion visual evoked potential," *IEEE Trans. Neural Syst. Rehabil. Eng.*, vol. 30, pp. 85–95, 2022.

[47] Y. Pei et al., "A tensor-based frequency features combination method for brain–computer interfaces," *IEEE Trans. Neural Syst. Rehabil. Eng.*, vol. 30, pp. 465–475, 2022.

[48] J. Jiang, C. Wang, J. Wu, W. Qin, M. Xu, and E. Yin, "Temporal combination pattern optimization based on feature selection method for motor imagery BCIs," *Frontiers Hum. Neurosci.*, vol. 14, p. 231, Jun. 2020.

[49] Y. Pei et al., "Data augmentation: Using channel-level recombination to improve classification performance for motor imagery EEG," *Frontiers Hum. Neurosci.*, vol. 15, Mar. 2021, Art. no. 645952.

[50] H. Altaheri, G. Muhammad, and M. Alsulaiman, "Physics-informed attention temporal convolutional network for EEG-based motor imagery classification," *IEEE Trans. Ind. Informat.*, vol. 19, no. 2, pp. 2249–2258, Feb. 2023.